

HOW TO CALCULATE THE GEOMETRY OF VORTEX RIPPLES

Ken Haste Andersen¹ and Jørgen Fredsøe²

Abstract: The topic of this paper is the calculation of the wave length and the profile of fully developed vortex ripples. A computational model of the flow and sediment transport over vortex ripples has been constructed, which makes it possible to perform morphological calculation of vortex ripples. Using a stability analysis of the fully developed ripples, the minimal wave length of the ripples is calculated. This minimal wave length was found to depend on the settling velocity only. The profile of the ripples are calculated, and the steepness is found to depend upon the Shields parameter and the settling velocity.

INTRODUCTION

In the coastal zone, the appearance of ripples on the bed is ubiquitous, occurring at shear stresses even smaller than the critical shear stress for grain movement on a flat bed, up to sheet flow conditions. The ripples modify the conditions near the bed such that the flow and sediment transport is qualitatively different from the conditions on a flat bed. A description of the flow and sediment transport over a rippled is therefore an important boundary condition in models

¹Department of Hydrodynamics and Water Resources (ISVA), the Danish Technical University, building 115, DK-2800 Lyngby, Denmark. kenand@isva.dtu.dk.

²Professor, ISVA. jf@isva.dtu.dk.

of the coastal environment. The flow and sediment transport is determined by the geometry of the ripples, i.e. the length and the height, and the assessment of these is the topic of the present paper.

Ripples created by gravity waves fall into two categories: rolling grain ripples and vortex ripples. The rolling grain ripples are a transient phenomena arising when ripples are formed on a flat bed. The initiation of rolling grain ripples have been described by Blondeaux (1990) and Vittori & Blondeaux (1990) using a fluid mechanical instability, and by Andersen (1999) by a granular model. The rolling grain ripples are not interesting for the coastal engineer as they are not stable (Stegner & Wesfried 1998, Scherer *et al.*, 1999) and always develop into the predominant ripples in the coastal zone: the vortex ripples (hereafter all references to the ripples refer to vortex ripples). The physics behind the wave length selection of the rolling grain ripples are very different from that of the vortex ripples. The results from the rolling grain ripples can therefore not be used for the vortex ripples.

Since the seminal work of Bagnold (1946), there has been many measurements of the geometry of the ripples (for a compilation see Nielsen, 1981). The theoretical understanding of the mechanism behind the selection of wave length and the geometry of the ripples is however scarce. The only attempt at building a model of the fully non-linear ripples is the simple model of Fredsøe & Brøker (1983).

The aim of the present paper is to show some of the basic mechanisms behind the selection of the ripple length and how the ripple profile is formed. To this end a computational model has been constructed. The idea have been to keep the setup in the model as simple as possible to facilitate a clean description of the dynamics of the ripples.

THE COMPUTATIONAL MODEL

The model consists of a ripple profile with one or more ripples on the bottom of a channel. The boundaries on the sides are periodic such that the calculation is performed on an infinite train of ripples. The simulation is made in a duct of height $2D$ which is accomplished by having a symmetry line at $y = D$ (i.e. the vertical gradient of all quantities is zero; $\partial/\partial y = 0$ at $y = D$).

The model consists of three parts: the flow model, the sediment transport model and the morphological module. For a detailed description of the model see Andersen (1999).

The Flow Model

The flow is described by the Reynolds-averaged Navier-Stokes equations which is driven by an oscillating pressure gradient added all over the domain.

This is an artificial way of simulating real waves, which is similar to performing experiments in an U-tube. This way only the horizontal part of the orbital motion is resolved, and the streaming in the bottom boundary layer is not resolved.

The flow is regarded as fully turbulent and to resolve the turbulence the k - ω model of Wilcox (1988) is used. The k - ω model consists of a transport equation for the turbulent kinetic energy k and the dissipation of the turbulent kinetic energy ω :

$$\frac{Dk}{Dt} = \frac{\partial}{\partial x_j} \left[(\nu + \sigma^* \nu_t) \frac{\partial k}{\partial x_j} \right] - \overline{u_i u_j} \frac{\partial U_i}{\partial x_j} - \beta^* k \omega \quad (1)$$

$$\frac{D\omega}{Dt} = \frac{\partial}{\partial x_j} \left[(\nu + \sigma \nu_t) \frac{\partial \omega}{\partial x_j} \right] + \gamma \frac{\omega}{k} \left(-\overline{u_i u_j} \frac{\partial U_i}{\partial x_j} \right) - \beta \omega^2, \quad (2)$$

where

$$\frac{D}{Dt} \equiv \frac{\partial}{\partial t} + U_j \frac{\partial}{\partial x_j}. \quad (3)$$

The eddy viscosity is calculated as:

$$\nu_t = \gamma^* \frac{k}{\omega} \quad (4)$$

and the closure coefficients are given as (Wilcox, 1993):

$$\begin{aligned} \gamma^* &= 1, & \gamma &= 5/9 & \beta^* &= 9/100 \\ \beta &= 3/40 & \sigma &= 1/2 & \sigma^* &= 1/2. \end{aligned}$$

This model is similar to the popular k - ϵ model but has two improvements: 1) it is possible to integrate through the viscous sub-layer without dubious damping-functions, thus avoiding the use of wall-functions (Patel and Yoon, 1995), 2) the model is known to perform better in flows with strong adverse pressure gradients (Wilcox, 1993), which is exactly the case for the wave boundary layer. Furthermore the boundary conditions on the bed for k and ω are simple and make it possible to account for both smooth and rough bed conditions. The k - ω -model has previously been used with success to calculate the flow over dunes in rivers (Yoon and Patel, 1996).

The details of the numerical solution of the model can be found found in Andersen (1999) and Tjerry (1995), but the main points will be briefly mentioned. The Reynolds-averaged Navier-Stokes equations are solved using a finite volume code. The discretization in space is made using the high order limiter scheme ISNAS (Zijlmea, 1996), which is similar to the classical QUICK scheme by Leonard (1979). The discretization in time is implicit with the higher order spatial terms

made semi-explicit to retain a 5-cell stencil, and the pressure is solved using the PISO algorithm (e.g. Versteeg and Malalasekera, 1995).

The flow model was validated against measurements of the velocity profile over a rippled bed.

The Sediment Transport

The sediment transport is divided into two partitions, the bed load and the suspended load.

The bed load is described using the Engelund-Fredsøe formula (1976). This formulation is similar to the well known Meyer-Peter formula, but it has corrections to avoid over-estimation of the transport at high shear stress rates, and it also provides a compatible boundary condition for the suspended sediment. For details of the bed load formula and the bed boundary condition used see Fredsøe & Deigaard (1992) and Andersen (1999).

The bed load flux q_b is a function of the slope of the bed and the Shields parameter defined as

$$\theta \equiv \frac{\tau_b}{\rho g(s-1)d} \quad (5)$$

where τ_b is the shear stress on the bed, ρ is the density of the water, s ($= 2.65$) the relative density of the sediment, g the gravitational acceleration and d is the grain diameter.

The suspension is modelled as an advection diffusion process of the concentration of suspended sediment c :

$$\frac{Dc}{Dt} = w_s \frac{\partial c}{\partial y} + \nabla(\epsilon_s \nabla c), \quad (6)$$

where w_s is the settling velocity and $\epsilon_s = \nu_T$ is the diffusivity of the suspended sediment. The bed boundary condition is a reference concentration at $y = 2d$ given as a function of the Shields parameter.

The flux of sediment is made non-dimensional as:

$$\phi_b = \frac{q_b}{\sqrt{g(s-1)d^3}} \quad (7)$$

$$\phi_s = \frac{1}{\sqrt{g(s-1)d^3}} \int_{y=h(x)}^D uc dy. \quad (8)$$

The Morphological Module

When the flow and the sediment transport has been calculated it is, at least

in principle, simple to make a morphological calculation where the bed profile is continuously changed. The change in the bed profile can be found using the continuity equation for the sediment

$$\frac{\partial h(x, t)}{\partial t} = -\frac{1}{1-n} \frac{\partial q_t(x, t)}{\partial x}, \quad (9)$$

where n ($= 0.4$) is the porosity of the bed and $q_t = q_b + q_s$ is the total sediment flux.

If the slope of the bed exceeds the angle of repose (33°) then an avalanche sets in. This is simply modelled by a strong down slope flux of bed load.

The continuity equation is discretized using the QUICK scheme of Leonard (1979) which is third order accurate in space. To avoid numerical instabilities the sediment transport is smoothed using an ordinary running average. In principle the bed can be updated every time step using the continuity equation, but in practice this requires that acceleration terms due to the moving grid are incorporated in the governing equations (e.g. Mayer 1997). Instead a more pragmatic approach has been adopted – the bed is only updated every tenth time step. This way the solver is “kicked” every time the bed and the grid are updated, but after ten time steps it has recovered completely. Usually 3000 time steps per period have been employed for morphological calculations.

THE FLOW OVER RIPPLES

The flow over a rippled bed can be characterised by five non-dimensional parameters: λ/a , h/λ , k_N/D and Re_a . Here λ and h is the ripple length and height, k_N is the Nikuradse roughness of the bed, D is the depth and $Re_a = U_m a/\nu$ is the Reynolds number with a being the amplitude of the oscillatory motion and U_m the maximum velocity away from the bed. The Reynolds number and the relative roughness is of minor importance, and if $D > 15h$ it has been found that the flow is nearly independent upon the depth (Andersen, 1999). This leaves only two important parameters, the length and the steepness of the ripples λ/a and h/λ .

The flow over ripples is dominated by the movement of vortices over the ripples. The snapshots in figure 1 clearly shows the formation of the separation bubble early in the wave period. The bubble has a very strong rotation, with velocities near the bed on the order of the free stream velocity. The bubble grows quickly from the crest of the ripple, and reaches the maximum length shortly after the outer flow begins to decelerate. At this point the length of the bubble is a little less than a . When the flow decelerates, the bubble is “curling up” into the main flow, but still maintaining the strong rotation. Shortly after the main flow has reversed, the bubble is lifted over the crest and ejected into the flow, thus becoming a free vortex ($\omega t = 30^\circ$). It is hard to see the ejected vortex in

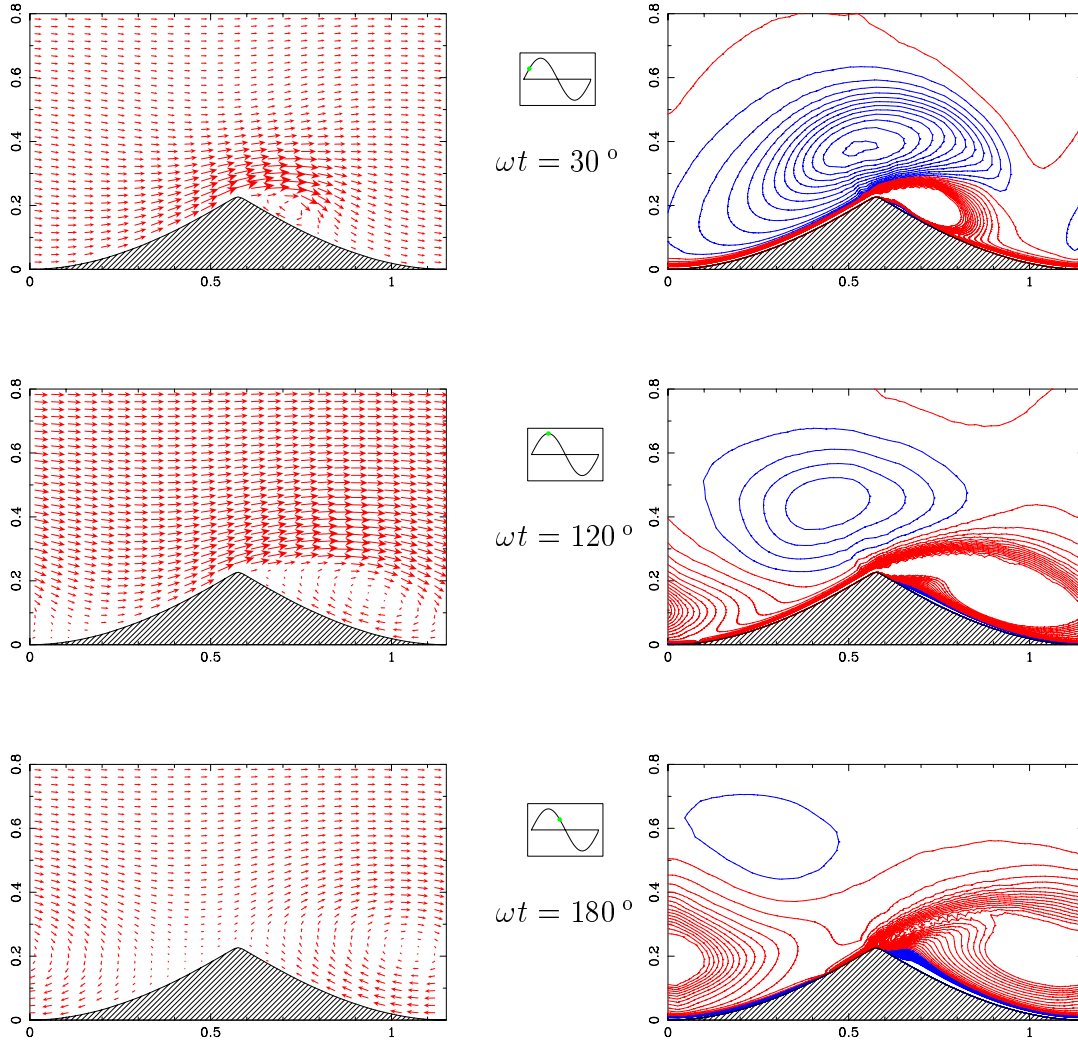


Figure 1: The flow over a fixed ripple at three instants during the first half of the wave period. To the right is a vector plot of the velocity field, and to the left the curl of the velocity field. The contours have been cut off in areas of very high “vorticity”, and these are the blank areas in the middle of the separation bubble ($\lambda/a = 1.2$, $h/\lambda = 0.2$).

the vector plots where it only manifests itself as a fluctuation in the velocity field, but on the plots of the average vorticity it is evident. The vortex travels far over the ripple, and when the flow reverses again it has travelled almost two ripple lengths, or more than two times a . When the next vortex is shed into the flow, the vortex ejected at the end of the previous half period is almost dissipated.

THE SEDIMENT TRANSPORT OVER RIPPLES

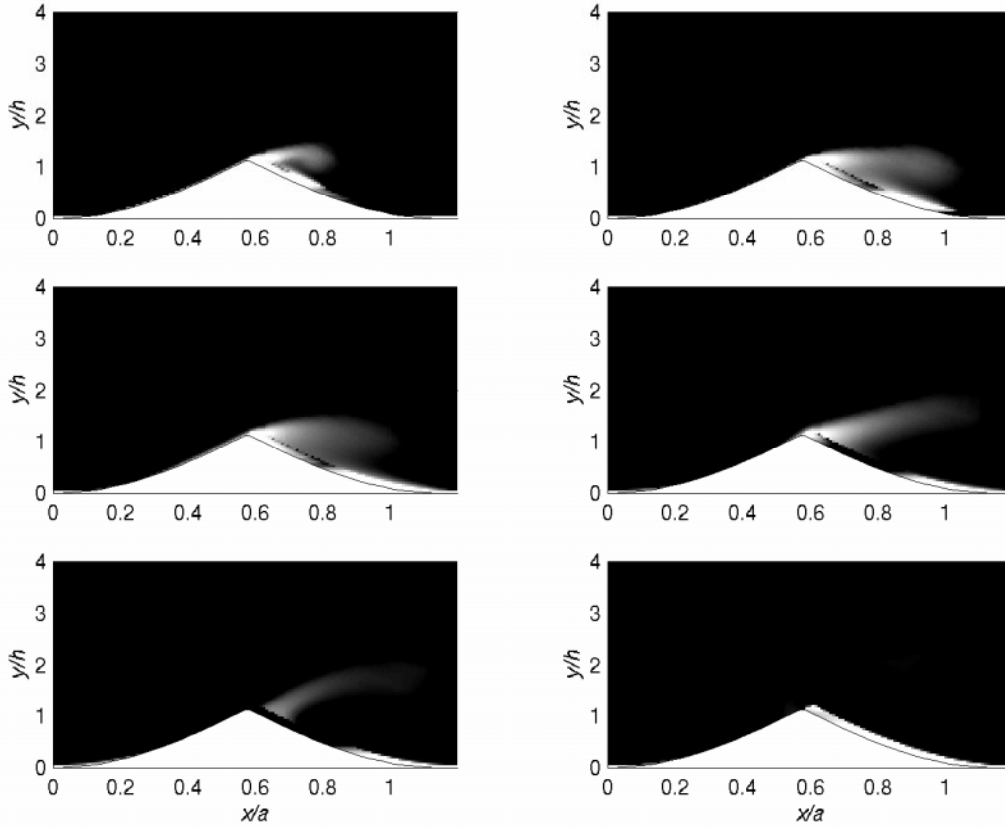


Figure 2: The transport of suspended sediment over a ripple at six snapshots ($\omega t = 30^\circ$ to 210°). The flow is the same as in figure 1. The scale show the log of the concentration of suspended sediment – the lighter, the higher concentrations of sediment (test case one, $\lambda/a = 1.2$, $h/\lambda = 0.20$).

When the sediment transport is considered, two more non-dimensional parameters enter the problem, namely the maximum Shields parameter on a flat bed (θ') and the relative settling velocity w_s/U_m .

The sediment transport over ripples is illustrated through two test cases. The maximum Shields parameter on a flat bed for both test cases is $\theta' = 0.15$, which is reasonably low, but still far above threshold. Two values of the settling velocity have been used: $w_s/U_m = 0.185$ and 0.065 . The high settling velocity correspond to a regime with almost no suspension (test case one), and the low settling velocity correspond to a regime which is dominated by suspension (test case two).

Snapshots of the suspended sediment in the first half period for the two test cases (figure 2 and 3) show the large effect of changing the settling velocity. Even though the total amount of sediment in suspension is markedly different the general features are similar. A strong jet of sediment is thrown over the

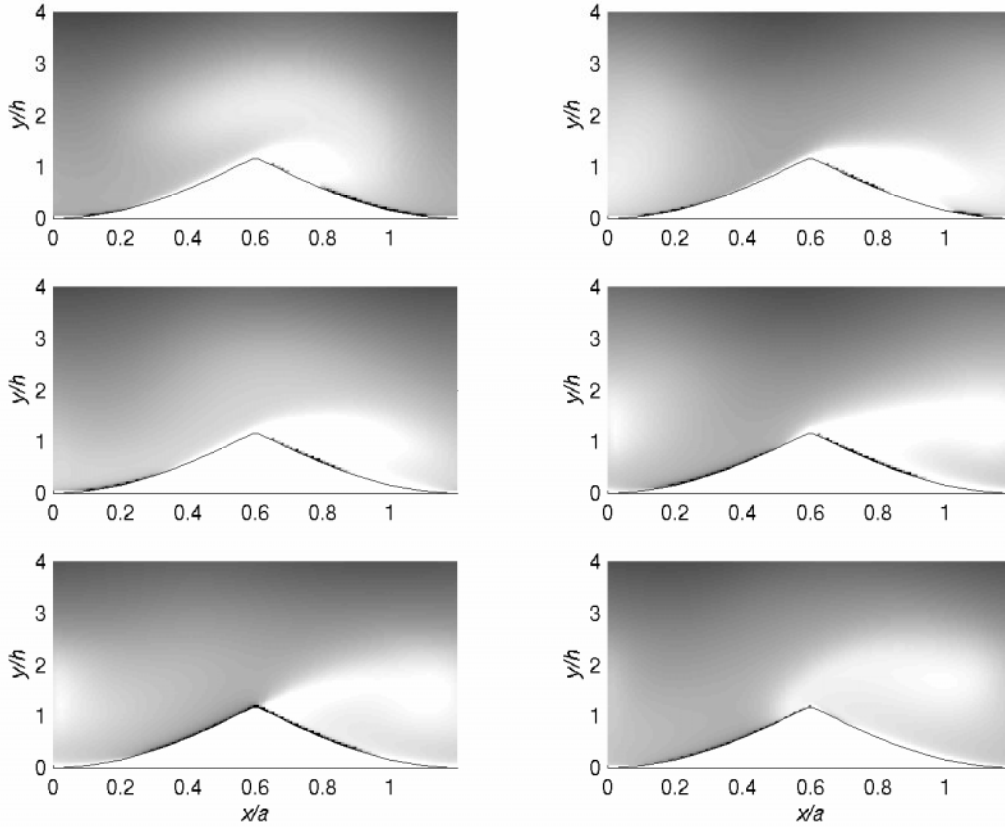


Figure 3: As figure 2, but with $w_s/U_m = 0.065$ (test case two).

crest of the ripple, on top of the separation bubble. When the flow reverse this jet follow the separation bubble over the crest. In test case one the settling velocity is so large that the sediment settles almost immediately after this, while in test case two the cloud of sediment can be followed as it is advected with the flow. Another feature which is similar in both cases is the large concentrations of sediment which is seen close to the bed, particularly inside the separation bubble. This transport is dominating the total suspended load in test case one, while the suspension in the jet dominates in test case two. The suspended sediment in test case one can then be said to be more dominated by the local shear stress, almost like an extension of the bed load, while the transport is dominated by advection in test case two. The two modes of suspension have been labelled the near bed suspension and the advected suspension respectively.

Averaging the sediment transport over one period, the effect on the ripples is seen (figure 4). The bed load is the same for both test cases, and in general it is seen that there is an average transport of bed load towards the crest. The effect of the bed load is therefore to bring sand from the trough to the crest of the ripple, where it again falls down as avalanches on the sides of the ripple. For the first test

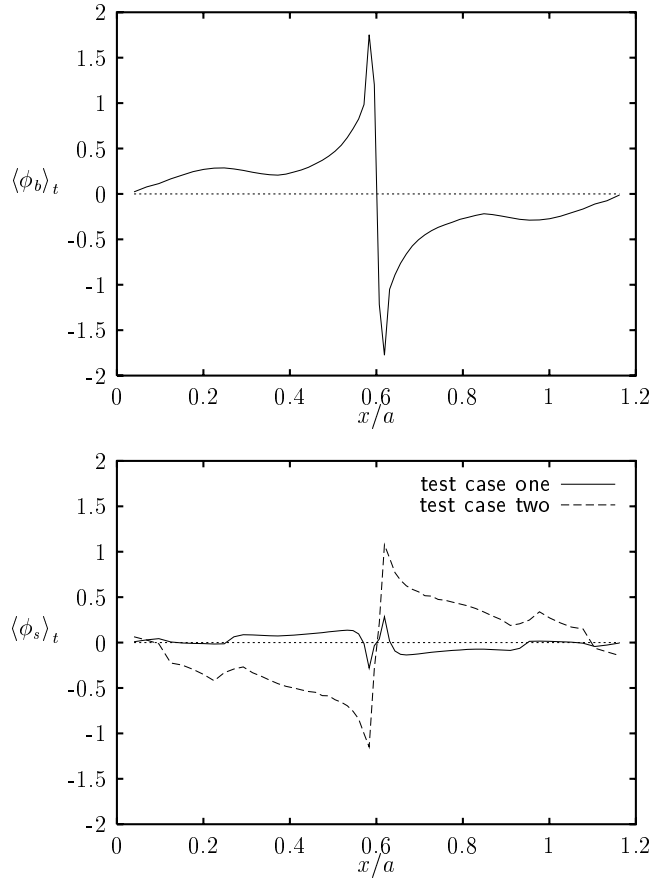


Figure 4: The sediment transport averaged over one wave period for the two test cases. Top: bed load, bottom: suspended load ($\lambda/a = 1.2$, $h/\lambda = 0.2$).

case the suspension is dominated by near bed suspension, which is transported by the near bed flow like the bed load. The average suspension is therefore also directed towards the crest of the ripple. In test case two the advected suspension dominate which result in the average suspension being directed away from the crest. The advected suspension therefore tends to destabilise the ripple.

STABILITY ANALYSIS

The dynamics of the ripples and the mechanics behind the selection of wave length has been analysed in more detail using a stability analysis of the fully developed profiles. The idea is to have two identical ripples in a periodic domain, except that one of the ripples is perturbed. When the morphological model is run with these initial conditions two things can happen: either the two ripples are unstable, i.e. the perturbed ripple will be taken over by the unperturbed ripple and diminish, or they will be stable and the perturbed ripple can grow and the two ripples will end up with equal size. The minimal stable wave length is where

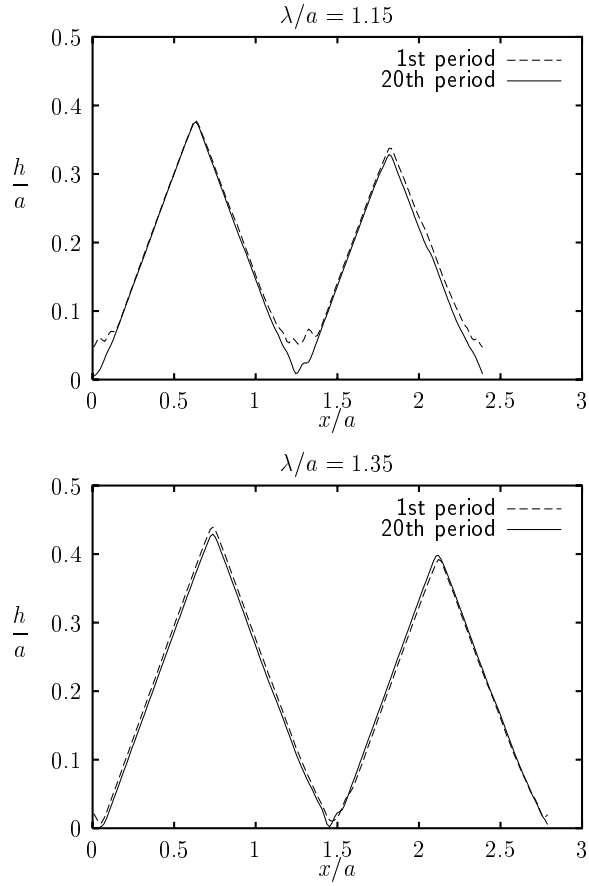


Figure 5: The evolution of two non-equal ripples from morphological calculations ($\theta' = 0.50$, $w_s/U_m = 0.185$).

there is a cross over between stability and instability.

An example of such an analysis is seen in figure 5. Here the ripple lengths are $\lambda/a = 1.15$ and 1.35 . The flow conditions are $\theta' = 0.50$ and $w_s/U_m = 0.185$ – a bed load dominated regime. The right ripple is perturbed by making it 10 % smaller than the left ripple. Two different behaviours are observed: in the case where $\lambda/a = 1.2$, the smaller ripple is slowly being eaten by the larger ripple. In the other case the two ripples are stable, and the smaller ripple slowly grows. The minimal wave length is therefore to be found in between the examples, so $\lambda_m = 1.25$.

The analysis have been conducted for $\theta' = 0.15$ and $\theta' = 0.50$ over a range of settling velocities (figure 6). The results are somewhat surprising. The minimal wave length could take two values: for settling velocities $w_s > 0.070U_m$ the selected wave length were $1.25a$. This corresponds to a regime dominated by bed load and near-bed suspension. For $w_s < 0.070U_m$ there is a transition

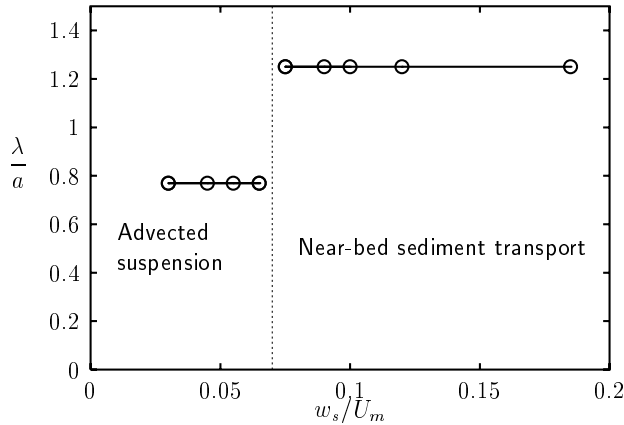


Figure 6: The variation of the minimal wave length as a function of the settling velocity for $\theta' = 0.15$ and $\theta' = 0.50$.

to a smaller wave length, due to a dominance of the advected suspension. The minimal wave length did *not* depend upon the Shields parameter. The transition point ($w_s/U_m = 0.070$) corresponds well with the transition between a one dimensional ripple pattern and a two dimensional ripple pattern as measured by Nielsen (1979).

The relation between the minimal wave length (λ_m) calculated above and the most probable wave length in a ripple pattern is not a trivial question. The minimal wave length sets the shortest possible length of the ripples. If a train of ripples is squeezed so that the length of one or more of the ripples become shorter than λ_m then that (or these) ripples will be annihilated and the train of ripples will adjust to a new average wave length. This length will, however, be larger than λ_m . The average length can be made shorter if one of the ripples spontaneously create a new ripple or if a defect invades into the pattern. The defects present in the ripple pattern is therefore responsible for pushing the pattern towards the minimal wave length. The density and motion of the defects is the topic of further studies.

It should be noted that λ_m is relatively large compared to measurements of ripple lengths (Nielsen, 1981). This might be attributed to the presence of defects in the ripple pattern during the measurement. The measurements of the ripple length is often performed by taking a transect of a two-dimensional rippled bed and then defining the wave length as the length of the transect divided by the number of ripples. If there is a defect in the transect this will show up as a short ripple, with the result that the wave length is being underestimated. The measurement is therefore a combined measurement of the wave length and the

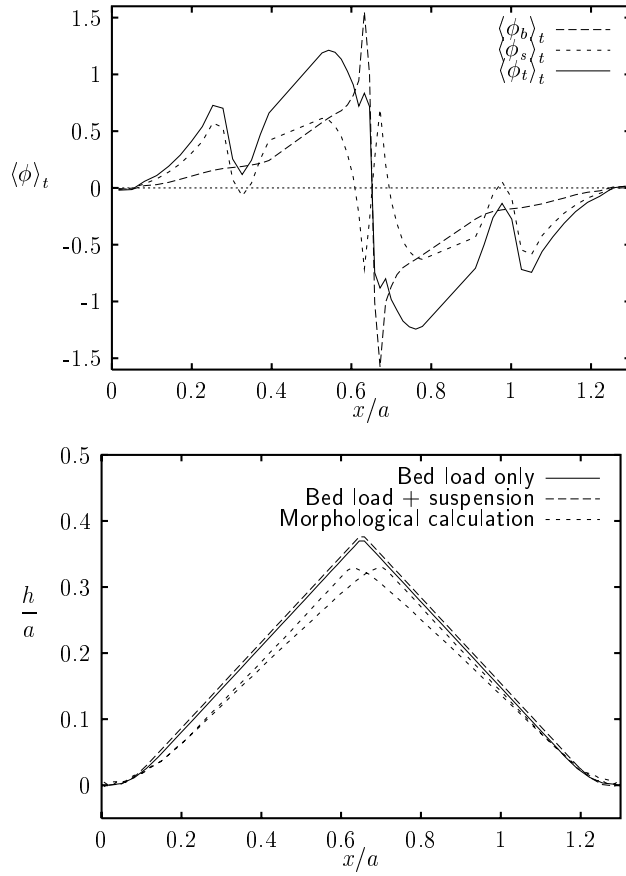


Figure 7: The sediment transport averaged over one period without avalanche correction (top) and the resultant profiles compared with the profiles from a morphological calculation (bottom). The profile from the morphological calculation the profile is shown in the two extreme positions. ($\theta' = 0.15$, $w_s/U_m = 0.10$).

density of defects in the profile.

THE RIPPLE PROFILE

The equilibrium profile of vortex ripples has been the topic of some interest, one of the reasons for the interest being that the steepness is important for the friction.

The ripple profile can be calculated by brute force using a morphological calculation. It can also be calculated using the sediment transport over a ripple averaged over one wave period. This is the basic concept behind the simple model of the ripple profile developed by Fredsøe & Brøker (1983). The idea is to find the profile that has a zero transport averaged over one period, i.e.

$$\langle \phi_b(x, t, h_x) + \phi_s \rangle_t = 0 \quad (10)$$

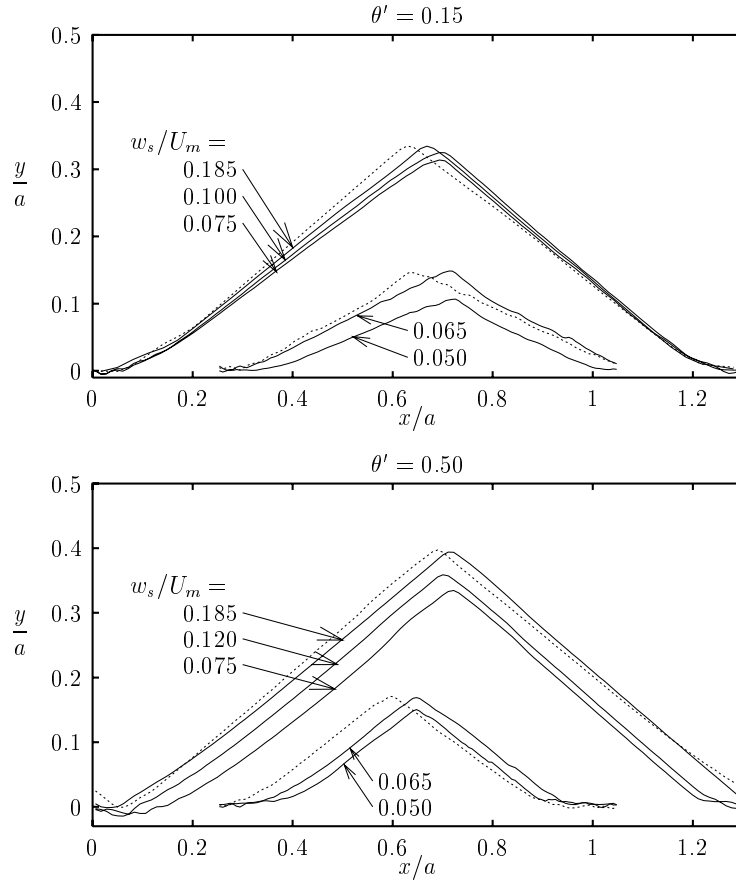


Figure 8: The equilibrium profiles for ripples with $\theta' = 0.15$ (top) and $\theta' = 0.50$ (bottom) and varying the settling velocity from $w_s/U_m = 0.185$ to 0.050 . The profiles are shown at the end of the first half period, but two profiles ($w_s/U_m = 0.184$ and 0.065 , stippled lines) are shown at the end of the second half period to illustrate the movement of the profile during the period.

for all x , where h_x is the bed slope. The bed load is a function of the slope of the bed through the gravity correction. If the shear stress on the bed and the suspension is known Eqn. (10) can be solved for $h_x(x)$, which in turns can be integrated to find $h(x)$. In the model of Fredsøe & Brøker (1983) a plausible assumption of the shear stress and the suspension is made, and from that the profile is calculated. In the bed load only case, it was found that almost any reasonable assumption gives a very triangular profile. By adding suspension Brøker (1985) found corrections to the profiles which reduced the steepness of the ripples.

Using a fixed profile the shear stress and the suspension have been calculated for $\theta' = 0.15$ and $w_s/U_m = 0.10$ (figure 7, left). Solving (10) gives the profiles shown in figure 7, bottom. The profiles are almost triangular except for a small

rounded trough reflecting the fact that a major part of the profile is shaped by avalanches. As this method does not resolve the back and forth motion of the crest, the resultant steepness is too large, but apart from that there is not much difference between the simple calculation and the full numerical solution.

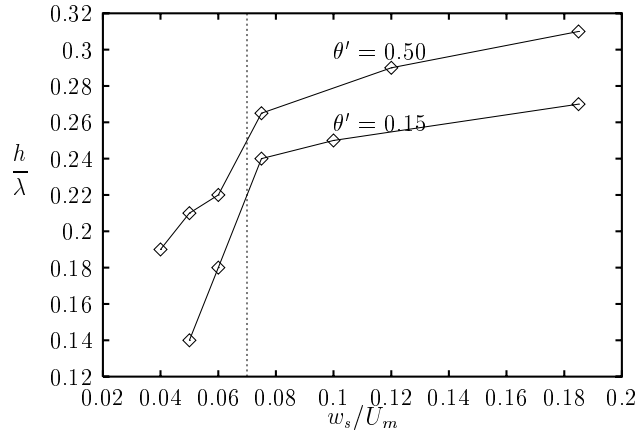


Figure 9: The steepness of the ripples as a function of the settling velocity.

Using the morphological calculations the ripple profiles have been calculated for $\theta' = 0.15$ and $\theta' = 0.50$ for a wide range of settling velocities (figure 8 and 9). In all the cases in the regime dominated by bed load and near-bed transport the ripples are very triangular, but they become slightly less steep as the settling velocity is lowered. This might be partly due to a larger back and forth motion of the crest as the sediment transport is increased, which gives rise to a less steep ripple.

The ripples are in general steeper than could be expected from measurements (see e.g. Nielsen, 1981). The discrepancy might partly be attributed to a too large angle of repose used in the calculations (33°). As there is constantly motion on the sides of the ripples the packing will be loose, and they can not be expected to reach the static angle of repose. In fact, Stegner & Wesfried (1998) found that the angle of repose on the ripples were 27 to 15 % lower than the static angle of repose. This means that the steepness calculated here are overestimated with approximately 20 to 30 %.

CONCLUSION AND ACKNOWLEDGEMENTS

The minimal wave length of vortex ripples were calculated, and it was found that there is a cross-over between two different wave lengths, determined by the settling velocity. The profiles of the ripples were very triangular with sides the angle of repose, but showed a decline in steepness when the settling velocity were reduced or the Shields parameter increased.

This study was partially funded by the Commission of the European Communities, Directorate-General XII for Science, Research and Development Program Marine Science and Technology Contract No. MAS3-CT97-0115 (SEDMOC) and by the project “Intermediate Scale Coastal Behaviour: Measurement, Modeling and Prediction” under the NICOP programme sponsored by the US Navy, Office of Naval Research – Grant No. N00014-97-1-0792.

References

- Andersen, K. H. (1999). *Ripples Beneath Surface Waves and Topics in Shell Models of Turbulence*. PhD thesis, the Niels Bohr Institute, Copenhagen University.
- Bagnold, R. A. (1946). Motion of waves in shallow water, interaction between waves and sand bottoms. *Proc. R. Soc. London, Ser. A*, 187:1–15.
- Blondeaux, P. (1990). Sand ripples under sea-waves. part 1. ripple formation. *Journal of Fluid Mechanics*, 218:1–17.
- Engelund, F. and Fredsøe, J. (1976). A sediment transport model for straight alluvial channels. *Nordic Hydrology*, 7:293–306.
- Fredsøe, J. and Brøker, I. (1983). Shape of oscillatory sand ripples. *Progress Reports from ISVA, the Danish Technical University*, 58:19–29.
- Hedegaard, I. B. (1985). Wave generated ripples and resulting sediment transport in waves. Series Paper 36, ISVA, The Danish Technical University.
- Leonard, B. (1979). A stable and accurate convective modelling procedure based on quadratic upstream interpolation. *Computer Methods in Applied Mechanics and Engineering*, 19:59–98.
- Mayer, S., Garapon, A., and Sørensen, L. S. (1998). A fractional step method for unsteady surface flow with applications to non-linear wave dynamics. *International Journal for Numerical Methods in Fluids*, 28:293–315.
- Nielsen, P. (1979). Some basic concepts of wave sediment transport. Series paper no. 20, ISVA, the Danish Technical University.
- Nielsen, P. (1981). Dynamics and geometry of wave-generated ripples. *Journal of Geophysical Research*, 86(C7):6467–6472.
- Patel, V. C. and Yoon, J. Y. (1995). Application of turbulence model to separated flow over rough surfaces. *J. Fluids Engineering*, 117:234–241.
- Scherer, M. A., Melo, F., and Marder, M. (1999). Sand ripples in an oscillating annular sand-water cell. *Physics of Fluids*, 11(1):58–67.

- Stegner, A. and Wesfreid, J. E. (1998). Dynamical evolution of sand ripples under water. Submitted to Physical Review Letters.
- Tjerry, S. (1995). *Morphological calculation of dunes in alluvial rivers*. PhD thesis, ISVA, the Danish Technical University.
- Versteeg, H. K. and Malalasekera, W. (1995). *An Introduction to Computational Fluid Dynamics*. Longman Scientific and Technical.
- Vittori, G. and Blondeaux, P. (1990). Sand ripples under sea waves. part 2. finite-amplitude development. *Journal of Fluid Mechanics*, 218:19–39.
- Wilcox, D. C. (1988). Reassessment of the scale-determining equation for advanced turbulence models. *AIAA Journal*, 26(11):1299–1310.
- Wilcox, D. C. (1993). *Turbulence Modeling for CFD*. DCW industries Inc.
- Yoon, J. and Patel, V. (1996). Numerical model of turbulent flow over sand dune. *Journal of Hydraulic Engineering*, 1:10–18.
- Zijlema, M. (1996). On the construction of a third-order accurate monotone convection scheme with application to turbulent flows in general domains. *Int. Journal for Numerical Methods in Fluids*, 22:619–641.